Stable Surface Plasmon Resonances in Small Alumina-Embedded Silver Clusters

Murilo H. Moreira[1,2], Emmanuel Cottancin[1], Michel Pellarin[1], Olivier Boisron[1], Varlei Rodrigues[2], Jean Lermé[1], Matthias Hillenkamp[1,2]*

[1] Institute of Light and Matter, University Lyon, University Claude Bernard Lyon 1, CNRS, UMR5306, Villeurbanne F-69622, France

[2] Institute of Physics Gleb Wataghin, State University of Campinas, Campinas, SP, 13083-970, Brazil

*matthias.hillenkamp@univ-lyon1.fr

KEYWORDS: Surface plasmon resonance, silver clusters, size effects, environment, semi-quantal simulations, jellium

ABSTRACT

Localized Surface Plasmon Resonances are ubiquitous for the characterization and in applications of noble metal nanoparticles. Their dependence on chemical composition, size, shape and environment is widely studied since decades but still many aspects are subject of controversy. In this article we experimentally investigate surfactant-free and mass-selected silver nanoparticles embedded in alumina matrices in the size range between several atoms and more than 4 nm diameter, spanning the whole range from large nanoparticles, accurately described by classical Mie theory, down into the range of quantum size effects. Strong and stable resonances are observed for all sizes down to less than 50 atoms, i.e. ~1 nm diameter, without significant line shift or broadening as a function of size. With the help of semi-quantal simulations, we identify all signals as surface plasmon resonances. The absence of peak shifts is rationalized as due to the dielectric oxide environment and the constant width of the resonances as a convolution of inhomogeneities in the local environment and inherent broadening due to Landau damping. We discuss our results in comparison to ligand-stabilized nanoclusters and rationalize the different contributions to the Hamiltonian describing the systems.

Introduction

Metal clusters and nanoparticles play an ubiquitous role in everyday science and technology. They are widely studied for their plasmonic [1], magnetic [2], spintronic [3], catalytic [4], imaging [5] or biosensing [6] properties. Their electronic structure, which defines their physico-chemical properties, not only depends on their chemical composition but also sensitively on their size [7, 8] and environment through chemical bonds at the interface [9]. It is thus of central importance to know (1) whether such clusters retain their metallic band structure with delocalized valence electrons and below which size their electronic structure becomes more molecular-like, with spatially and energetically localized orbitals and transitions; (2) how this electronic structure is influenced by the local environment of the particle; and (3) how to theoretically describe such strongly correlated many-electron systems and their optical response. This last point specifically includes the question of the degree of precision required for a correct reproduction of experimental results, i.e. the trade-off between the complexity of ab-inito methods and the simplicity of corrected solid-state approaches.

One of the most prominent fingerprints of the electronic structure of noble metal nanoparticles is their Localized Surface Plasmon Resonance (LSPR), a collective excitation where all delocalized valence electrons in the cluster oscillate coherently with respect to the ion cores in an external electric field. The LSPR gives rise to strong colors in colloidal solutions and stained glasses [10] and depends sensitively on the chemical composition, the size, the shape and the local environment of the particle. It is commonly established that for small clusters the electronic band structure fragments into molecular-like, spatially and energetically localized levels and instead of collective LSPRs one rather finds single-electron transitions [11, 12, 13]. In these cases, highly structured absorption spectra and the observation of fluorescence indicate a “molecular-like” or “non-

metallic" electronic structure [14, 15]. The LSPR is thus one way of tracking the size-dependent metal-insulator transition in metals [16].

The way how the transition between a metallic nanoparticle, with continuous electronic band structure, and a molecular-like system takes place and how this transition is influenced by the chemical environment is still highly debated today despite many years of research. Throughout the last decade an enormous amount of research has addressed the wet-chemical fabrication of passivated metal nanoclusters and the dependence of the electronic structure and optical response on the choice of ligands [9, 17, 18, 19, 20]. All these systems have in common that metal core and ligand shell form a hybrid system where often the interface disturbs the electronic structure and dominates the resulting optical response. Furthermore, due to the covalent bonds at the interface, the size of the core with metallic properties (delocalized electrons, collective plasmonic response etc.) is necessarily smaller than the volume occupied by metal atoms.

In our work we address intrinsic properties of metal clusters and nanoparticles, more precisely how the plasmonic response depends on size and how it is influenced by a dielectric environment. In this article we study a plasmonic benchmark system, silver nanoparticles embedded in alumina matrices, and investigate if and how the LSPR is sustained for smallest sizes. In order to discriminate from other influences, we work with physically prepared, surfactant-free particles and mass-select them prior to embedding them in the protective oxide matrix. We then interpret our findings with the help of semi-quantal simulations which permit correlating the spectroscopic response with collective electronic excitations. By showing evidence of plasmonic responses down to ~40 atoms we furthermore demonstrate the absence of covalent bonds between metal cluster and oxide environment.

Experimental

Silver nanoparticles are fabricated in the gas phase using a magnetron sputtering/gas aggregation source [21]. Pure silver cluster ions are generated in the gas phase using a home-built magnetron cluster source (based on the principle introduced by Haberland et al. [22]) and guided towards the deposition chamber. Time-of-Flight Mass Spectrometry (ToF-MS) is used for in-situ characterization of the cluster ions in the gas phase and shows no trace of cluster oxidation or other complexes.

Small clusters are fabricated following a log-normal size distribution and the large diameter tail of the distribution might dominate the spectral response of the deposited ensemble. In order to avoid this bias, we mass-select the cluster ions prior to deposition. Mass selection is achieved with a Quadrupole Mass Spectrometer (QMS, Extrel) operated at 440 kHz. Changing the control parameters of the QMS electronics (mass command, ΔM and ΔRes) allows adjusting the mean and width of the transmission window over a large size range, the low cut-off being limited to ~200 Ag atoms maximum. The lower and upper limits of transmitted masses have been carefully calibrated by placing the QMS between the cluster source and the ToF-MS. The uncertainty of the mass cut-offs increases from atomic precision at low masses to ±5 atoms for upper cut-off values above 300 atoms.

For larger sizes a narrow Gaussian diameter distribution is obtained and size selection is not necessary. For the largest sizes presented in this work, deposited without mass selection, the width of the distributions was measured by ToF-MS to $\langle d \rangle = 2.9 \pm 0.6$ and 4.3 ± 0.3 nm and confirmed by Transmission Electron Microscopy (TEM), as shown in the Supporting Information.

The kinetic energy of the clusters is adjusted to below 0.5 eV/atom in order to ensure soft-landing conditions with minimal fragmentation [23]. The cluster ions are neutralized after deposition by thermal electrons evaporated from a filament in the deposition chamber. The alumina matrix is evaporated in a commercial electron beam evaporator and co-deposited simultaneously at room temperature onto fused silica substrates. Our alumina matrices are porous (~70% density with respect to the solid [24]), which has to be taken into account in the numerical simulations (see below).

The nanoparticle concentration is controlled and adjusted so as to avoid inter-particle interactions with typical loadings of <1 vol.%. Samples were removed from vacuum after fabrication and measured in a Perkin-Elmer Lambda 900 spectrophotometer. Linearly polarized light (TM) at the Brewster angle was used to minimize Fabry-Perot interferences between the two alumina interfaces. In order to obtain a sufficient optical density for conventional UV-vis absorption spectroscopy, alumina films with embedded particles were typically between 1-2 μm thick.

Theory

The theoretical model used for the calculation of the optical excitation spectra has been described in detail elsewhere [25, 26, 27], a pedagogical and short (but complete) summary of the approach is given in the supplementary material of [8]. In short, the ionic background of the metal cluster is taken as spherical and continuous, jellium-like. Density functional theory (DFT) is used to describe the ground state, optical excitations are obtained within the Time-Dependent Local-Density-Approximation (TD-LDA). This description includes phenomenologically (but self-consistently) the absorption/screening properties of the ionic core background (effects related to the bulk

interband-transitions contribution) and the screening properties of the surrounding transparent matrix. In particular, the model describes self-consistently the interplay between the optical excitations and induced fields in the various media.

The conduction electrons of the metal particle, corresponding to the bulk s-p band, are responsible for the collective surface-plasmon excitation and for most of the (quantum) finite-size effects. They are quantum mechanically treated, whereas the spherical ionic background is approximated by a homogeneous positively charged distribution of radius R. We then describe the optical properties of the more localized d electrons through an additional homogeneous polarizable/absorbing dielectric medium characterized by a frequency-dependent complex dielectric function $\varepsilon_{ib}(\omega)$ and extending up to $R_1 = R - d$, where d is the skin thickness of reduced ion polarizability [25, 28, 29].

This self-consistent description accounts for all important contributions:

(1) the electronic spill-out, i.e. the extension of electron density beyond the jellium radius due to the finite depth of the confining Kohn-Sham potential;

(2) the silver surface layer of ineffective ion-core polarizability of thickness d;

(3) the surrounding dielectric matrix, including a possible local porosity and

(4) all the relevant finite-size quantum effects, in particular the non-locality of the electronic response.

The complex dielectric function of silver related to the interband transitions, $\varepsilon_{ib}(\omega)$, was extracted from experimental data [30] by a Kramers-Kronig analysis [31]. The bulk-alumina

dielectric function $\varepsilon_m(\omega)$ was taken from the same reference [30] and the values for porous alumina from Ref [24]. In the DFT-TDLDA approach, the computed spectra depend on a parameter δ entering the independent-electron Green's function. This parameter acts as a smoothing parameter which can be considered as introducing phenomenologically dissipative channels which are not included in the modelling (see supporting information of [8]) and consequently a finite life time and line broadening. It accounts, in the large size limit, for all size-independent effects and can, in this case, be identified with the bulk contribution to the line width. In this work we either fix δ to this large particle size limit value of 60 meV, consistent with classical Mie simulations using dielectric functions from the literature [30, 32], experimental data on larger particles [33] and all our recent publications, or adjust it empirically to reproduce the experimentally observed width of the absorption peak, as described below. The choice of δ is discussed in detail in the Supporting Information.

Results

We have measured the optical absorption spectra for mass-selected, alumina-embedded, surfactant-free silver clusters. In order to make sure that the large diameter tail of the log-normal size distribution, as produced in the cluster source, does not dominate the optical response of the ensemble, we select a specific interval of deposited sizes using a quadrupole mass filter. Fig. 1 shows the optical absorption spectra for sizes between more than 4 nanometer diameter and several atoms only, i.e. across the entire range from nanoparticles large enough to be described by classical Mie theory down to cluster deep in the range of quantum size effects [29, 34]. The absence of coalescence upon deposition was verified by Transmission Electron Microscopy of thin samples

deposited on TEM grids, fabricated under identical conditions. We furthermore estimate fragmentation during the deposition as negligible, as no signals from smallest clusters [34] or atoms [35] are observed in the energy range between 3 and 4 eV. We can thus unambiguously attribute the observed optical resonances to the corresponding size ranges stated in Fig. 1. Except for the smallest sizes (below 1 nanometer diameter), a clear surface plasmon resonance at ~2.9 eV, followed by the rise of the interband transitions in the further UV, is visible. Note that the variations in maximum energy between the shown spectra are of the same order as the variations between successive measurement of the same sample and are attributed to variations of local alumina environment across each sample. There is thus no evidence of clear size dependence of the plasmon resonance band (mean energy and width).

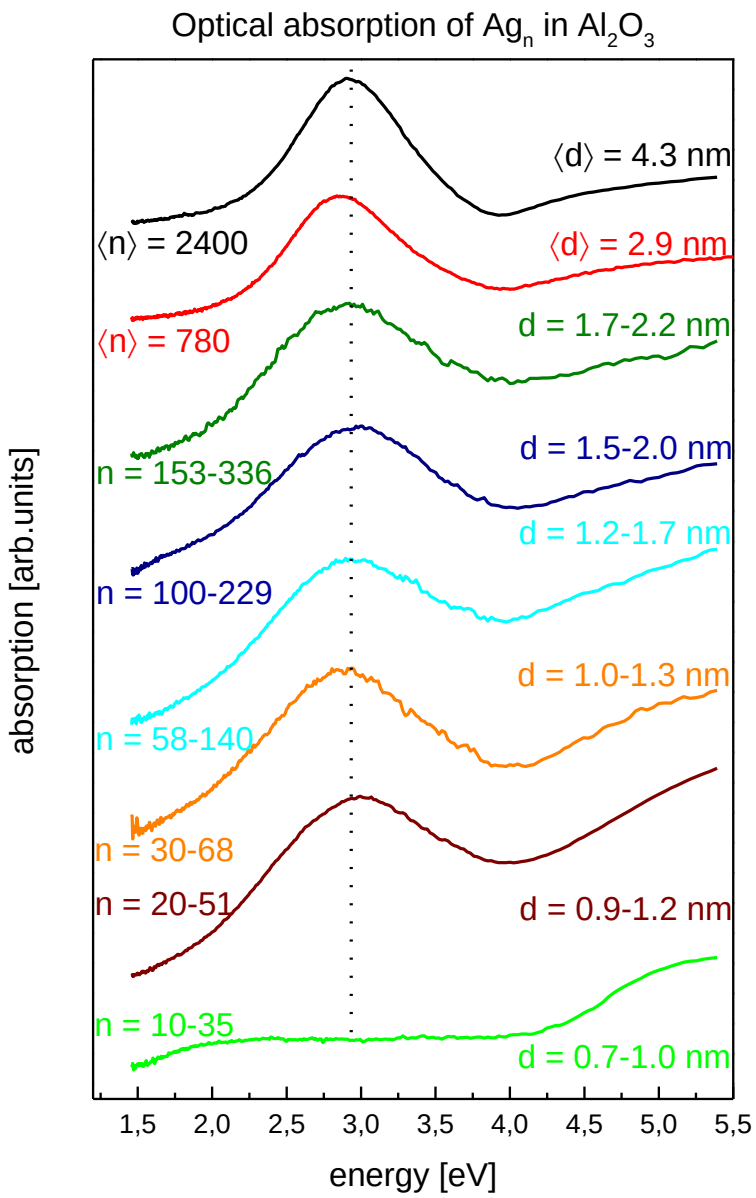

Figure 1. Optical absorption spectra for silver nanoparticles of varying size, embedded in alumina matrices. The topmost, black and red curves are for non-mass-selected ensembles centered on diameters of ⟨d⟩ = 4.3 and 2.9 nm, the other curves are for mass-selected distributions. The minimal and maximal numbers of atoms per particle transmitted through the mass spectrometer (n) and the corresponding diameters (d) are indicated.

We have furthermore verified the sample stability over time. Earlier work on silica-embedded silver clusters showed that these oxidize within several hours, with the sample color disappearing rapidly due to oxygen diffusion through the evaporated and porous glassy silica matrix [36, 8]. Alumina matrices, prepared under identical conditions, however, provide a much better protection against oxidation. Fig. 2 shows example absorption spectra measured over the range of 18 months without any sign of significant signal shift or loss. The slight differences are attributed to different probed positions on the sample. Even though our evaporated alumina matrices display significant porosity (70% density as compared to bulk alumina [24]), the permeability towards oxygen or water is much lower than in silica.

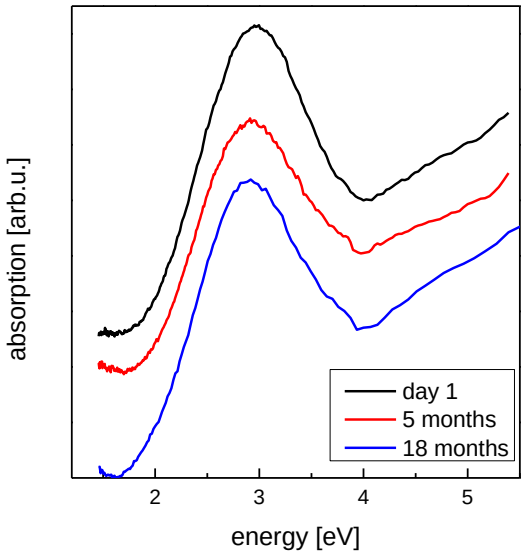

Figure 2. Temporal evolution of the optical absorption of the sample with n=153-336. No significant change in spectral position or width is detectable. The spectra have been scaled and shifted vertically for better comparison.

In order to verify if the intense peaks observed in the experimental spectra down to smallest sizes are consistent with a collective plasmonic excitation of the electron gas, we simulated the optical absorption for several sizes in the range between n = 40 and 2048. In order to avoid biasing effects both open and closed electronic shell structures are considered.

Fig. 3 shows the experimental spectra and the simulated counterparts, computed for a single but appropriate size and for two values of δ each time (see the theory section for the significance and practical effect of this smoothing parameter). A rather small δ value allows to resolve, in the small particle range, the fragmented pattern of the collective plasmon excitation. This fragmentation leads to a broadening of the band, reflecting the increasingly rapid decay of the plasmon with decreasing size into single electron-hole excitations, the so-called Landau damping [37]. When the size increases, the individual fragments bunch together in a narrow spectral range, gradually approaching a Lorentz profile with conspicuous shoulders (see e.g. Fig. 3b). Simulating the spectra with an increasingly large value for δ with decreasing size allows reproducing phenomenologically the experimental curves without changing the underlying electronic structures. The spectra shown were calculated for a porous alumina matrix [24]; simulations for other matrices are discussed in the supporting information.

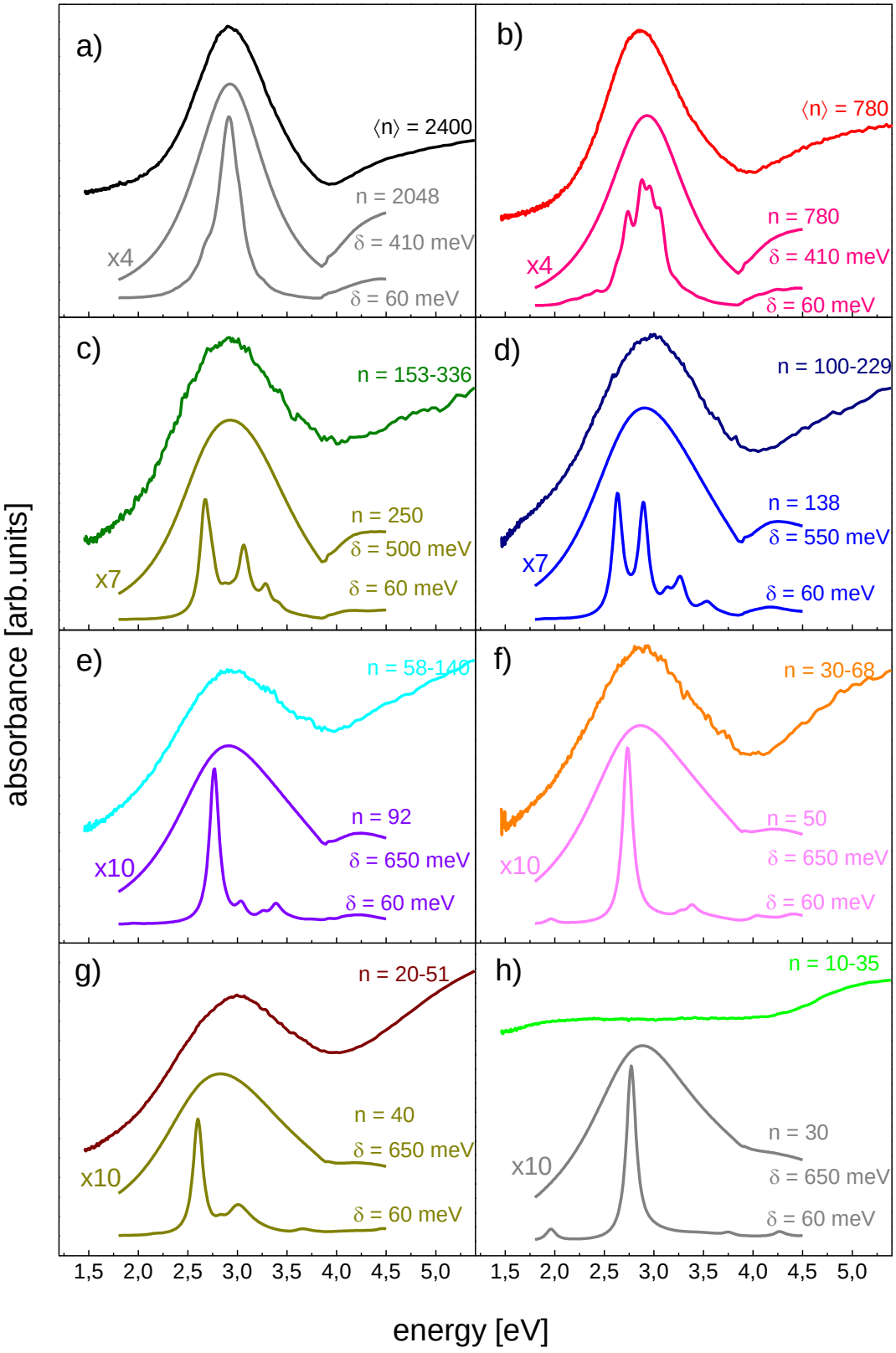
a)
⟨n⟩ = 2400
n = 2048
δ = 410 meV
x4
δ = 60 meV
b)
⟨n⟩ = 780
n = 780
δ = 410 meV
x4
δ = 60 meV
c)
n = 153-336
n = 250
δ = 500 meV
x7
δ = 60 meV
d)
n = 100-229
n = 138
δ = 550 meV
x7
δ = 60 meV
e)
n = 58-140
n = 92
δ = 650 meV
x10
δ = 60 meV
f)
n = 30-68
n = 50
δ = 650 meV
x10
δ = 60 meV
g)
n = 20-51
n = 40
δ = 650 meV
x10
δ = 60 meV
h)
n = 10-35
n = 30
δ = 650 meV
x10
δ = 60 meV
absorbance [arb.units]
1,5 2,0 2,5 3,0 3,5 4,0 4,5 5,0
1,5 2,0 2,5 3,0 3,5 4,0 4,5 5,0
energy [eV]

Figure 3. Comparison of experimental and simulated absorption spectra. In each figure the scaled experimental curve is shown at the top. The lowest curve is the simulated spectrum with fixed $\delta = 60$ meV, the intermediate one with δ adjusted to best reproduce the shape and width of the experimental curve. The curves with increased δ have been multiplied with a given factor for better comparison. The same values for δ as in e), f) and g) were used to simulate a curve for the smallest size (Fig. 3h).

Discussion

In view of the huge amount of literature treating the optical properties of noble metal clusters, the spectra in Fig. 1 are a further manifestation of how the environment crucially influences the collective electronic response of noble metal clusters. We now discuss our results in comparison with other works on gold and silver clusters (1) in a strongly (covalent) interacting environment, i.e. monolayer-protected nanoclusters and (2) in the gas phase and in very weakly interacting rare gas matrices.

The important role of the interface is most obviously seen in the vast literature on ligand-stabilized metal clusters [10, 38]. In that case the metal-insulator transition and thus the minimal size for the appearance of the LSPR is generally found for gold around sizes of 2 nm diameter, with the limiting size estimated in the range between 144-187 [11], ~279 [12] or 246-279 [13] atoms, highly dependent on the choice of surfactant molecule. The presence or absence of an LSPR strongly depends on the covalent bonds at the metal-ligand interface and the metallic core, in the sense that only a reduced fraction of gold atoms actually provides delocalized valence electrons to the LSPR. The ligand shell (and to a lesser degree the solvent in which the particles are dispersed)

also acts as dielectric environment to the plasmonic cores and thus influences the spectral position of the resonance. Much less is reported on ligand-stabilized silver nanoparticles, but the general observation of an LSPR appearing only above ~150 atoms diameter is consistent with the results on gold [39, 40].

The systems discussed here are different in the sense that the cluster surface is not saturated by covalent bonds. Some strong and localized bonds between metal and oxide cannot *a priori* be excluded, but the fact that strong absorption bands at the LSPR energy are observed down to less than 50 atoms rather supports a description of a metallic particle in an effective inert dielectric environment. Even slight oxidation has been demonstrated to rapidly disperse the oscillator strength across a very large spectral range [41], contrary to our experimental findings.

Previous studies have already shown that silver clusters in the gas phase [42, 43, 44] or supported on substrates [45, 46, 47] show a continuous blue shift of the LSPR with decreasing size. This size effect is, however, quenched in solid glassy matrices like photosensitive glass [35], silica [8] or alumina [25].

Our semi-quantal simulations of the absorption cross-sections of matrix-embedded silver clusters help us understand the differences between the various systems, the influence of the environment and the plasmonic behavior of the observed response. Two main quantum corrections to the classical Mie theory prediction occur when the size of the nanoparticle is reduced below ~3 nm diameter [8]. Spill-out, on the one hand, i.e. the extension of the electronic density beyond the atomic particle radius, leads to a red-shift of the LSPR, an effect, which is all the more important as the size decreases. A layer of reduced *d*-electron polarizability at the particle surface, on the other hand, results in a continuous blue-shift of the resonance with decreasing size [25, 28, 29].

This delicate balance, resulting in a net blue-shift for gas-phase clusters [42], is perturbed by the presence of a polarizable matrix due to screening effects. Not only is the classical Mie resonance shifted to smaller energies but the relative importance of the two opposite shifts is altered, leading in some cases to a complete quenching of size dependency.

In our case of alumina-embedded Ag clusters we find an overall absence of marked size-dependency (cf. Fig. 1). Depending on how the porosity of the evaporated matrix is described theoretically (overall mean porosity or dense matrix with a thin vacuum layer at the interface, see Supporting Information), a slight blue-shift may be seen in the simulations but it remains within the scatter of both simulated and experimental results. In contrast, the results differ significantly if the dielectric function for a dense bulk alumina is used (cf. Fig. S1). The dielectric effects of the surrounding alumina are thus correctly described in our model and in the following we focus on simulated spectra obtained for the porous matrix described above.

We next address the question whether the observed absorption bands can really be attributed to surface plasmon resonances. Recent Time-Dependent Density-Functional-Theory (TD-DFT) have shown that silver clusters down to 20 atoms display a concentration of oscillator strength in the spectral range of the LSPR, associated with spatial electron density oscillation typical of the surface plasmon excitation [15, 48, 49].

These theoretical findings, obtained from first principles/ab-initio calculations in which the atomistic structure of the particles is taken into account, are consistent with our less refined theoretical DFT-TDLDA calculations where the ionic background is described by a homogeneous structureless jellium. This approximation, which is all the more suitable the larger the cluster, allows explaining the observed findings within a very simple Hamiltonian theoretical framework. Such an approach, combined with the “Generalized Kohn’s Theorem” (GKT, also termed

"harmonic potential theorem" (HTP) in the literature) was described in detail in previous works [37, 50] but it is worthwhile summarizing the main prominent features. The implication of the GKT stems from the fact that the electron-jellium interaction potential is parabolic in the inner jellium volume ($V_{e-jel}(r < R) \propto r^2$). The total Hamiltonian can be split into three parts, describing, respectively: (1) the motion of the center-of-mass (CM) of the electron gas ($\boldsymbol{R}_{\mathrm{CM}}$ coordinate) and concomitantly –in view of the GKT- the electron gas oscillation as a whole (indeed the Hamiltonian H_{CM} describing the CM motion (i.e. the plasmon excitation) is that of a 3D isotropic harmonic oscillator); (2) the intrinsic -or relative- internal electron motions (coordinates $\boldsymbol{r}_i$) in the CM frame (the associated Hamiltonian H_{int} gives rise to a quasi-continuum of excitations); (3) the surface-induced coupling of the CM and intrinsic coordinates resulting from the spill-out, where the electron density tail probes the non-harmonic component of the electron-jellium interaction potential at the surface ($V_{e-jel}(r > R) \propto 1/r$).

Actually this coupling Hamiltonian (3) is responsible for the size-evolution (average 1/R behavior) of the characteristics of the plasmon excitation (shift and broadening of the LSPR band). In this Hamiltonian analysis the broadening/fragmentation of the LSPR band in the linear excitation regime can be straightforwardly interpreted in terms of a "discrete state coupled to a continuum": when the full Hamiltonian is taken into account, the eigen-wavefunction describing the CM motion, associated with the n=1 eigen-energy of the oscillator Hamiltonan H_{CM}, is "diluted", more precisely distributed, in a finite energy range. For large particle sizes, where the energy spectrum of the H_{int} Hamiltonian forms a quasi-continuum, the envelope of this distribution is Lorentzian. Since the electron gas - light interaction in the quasistatic regime writes as $W(t) \propto \mathbf{R}_{CM} \cdot \mathbf{E}(t)$, for small sizes, the plasmon excitation (CM motion) manifests itself in a fragmented absorption cross-section pattern (distinguishable peaks when a small δ value is used).

This fragmentation is in fact the direct signature of the "dilution" of the CM-wavefunction in the many-body energy spectrum of the full Hamiltonian. When the size increases the number of fragments increases drastically and moreover the fragments bunch together into a narrow continuous band (width $2\hbar\delta$), which can be considered as the classical quasistatic limit. In the jellium model used here, the decay of the plasmon excitation in the time domain therefore has to be attributed to its coupling, via the particle surface, to one-electron excitations (single particle-hole (p-h) transitions), a mechanism referred to as Landau damping. This mechanism is indeed the main dissipative decay channel of the collective plasmon excitation (lifetimes on the order of a few femtoseconds). It should be pointed out that, at least qualitatively, the physical pictures described above hold true also in the presence of dielectric media (surrounding matrix and interband dielectric medium) [37].

Note that the LSPR is highly sensitive to changes in cluster charge, shape or environment, which would continuously shift the resonance to lower or higher energies, depending on which parameter is changed. Bearing in mind this sensitivity, the agreement between experiment and simulations underlines the validity of our assumption of spherical and neutral particles.

In the frame of this description of the optical excitation, all our experimental and theoretical results are consistent. Even though the computed absorption spectra show considerable fragmentation, an underlying and collective center-of-mass motion, and thus a plasmon excitation, is still visible in the simulations, in good agreement with the experimental observations. We can consequently give a lower size limit of approximately 40 atoms for the persistence of surface plasmon resonances of silver clusters in both silica [8] and alumina matrices. Below this size no more LSPR is observed and we tentatively attribute this absence to chemical interface effects. Theoretical calculations show plasmon-like oscillations for gas-phase clusters down to 20 atoms

[49], in agreement with our semi-quantal simulations (cf. Fig. 3h), consequently we presume either charge transfer [51] or oxidation [41] as responsible for the plasmon quenching in very small oxide-embedded silver clusters.

Let us finally have a look at the widths of the experimental absorption peaks. Simple "limited mean free path" corrections to the classical Mie description of LSPRs predict an increasing peak width with decreasing cluster size, an argument that has also been rationalized within a quantum mechanical picture for a long time [1]. It is thus surprising that not only the mean experimental peak position but also its width do not change with size for silver clusters embedded in both silica [8] and alumina matrices. It is difficult to unambiguously define an accurate FWHM for the experimental curves, but values around 0.8-1.0 eV are found for the oxide-embedded particles, in agreement with previous data [52]. These values are considerably larger than for comparable clusters in rare gas matrices at very low temperature (0.3-0.5 eV) [15].

We have performed the same simulations as described above with elevated values for the δ parameter, in order to try to take into account phenomenologically the size- and possibly energy-dependent broadening effects of the individual excitations, as well as all the inhomogeneous broadening. The aim was to qualitatively reproduce the shape of the experimental absorption profiles. Fig. 3 shows the experimental absorption spectra, together with simulated spectra for δ = 60 meV and the width required for reasonable agreement. The simulations with δ = 60 meV are very useful as this value is a good compromise to visualize the fragmentation and as they describe the intrinsic contribution to line broadening via Landau damping. Satisfactory agreement is obtained for all sizes for increased values of δ (slight variations of the peak maximum between experiment and simulation are within the scatter of experimental reproductivity as well as of the scatter using different numerical descriptions for the matrix porosity). We note that the values of

δ needed in order to reproduce the experimental spectra increase with decreasing size. This observation allows a qualitative argumentation of consistency. As the cluster size decreases, the oscillator strength fragments over a certain spectral range, thereby broadening the resulting band. But at the same time less electrons participate in the optical excitation, and less transitions are possible. In the end, this leads, for very small sizes, to an overall reduction of spectral width over which the transitions are spread. This is best seen by comparing the simulated spectra for n = 780 and 50 at δ = 60 meV, where the apparent simulated FWHM decreases from 440 to 130 meV. In order to reproduce the experimental peak shapes, larger δ values are needed for smaller clusters.

The measured peak widths are significantly broader than for clusters in the gas phase or in rare gas matrices. In our case this cannot be attributed to inhomogeneous line broadening due to large size dispersions, we rather believe local inhomogeneities of the matrix to be mainly responsible for the overall broadening. It is furthermore reasonable to assume that the sensitivity to local environmental fluctuations increases with decreasing size as the degree of coordination decreases. In the simulations, these local environmental fluctuations lead to a line broadening, too, in addition to Landau damping inherent to our description. This is reflected in the larger scatter of calculated mean absorption energies for smaller cluster sizes if different descriptions of matrix porosity are considered, as shown in Fig. S1 of the Supporting Material. Empirically, we can thus reproduce the experimental curves in our simulations with increasing δ values for decreasing cluster sizes.

Conclusion

We have shown that alumina embedded silver clusters sustain surface plasmon resonances down to sizes around 1 nm diameter (<50 atoms). The samples are stable at ambient conditions for at least one year, contrary to ones with identical clusters embedded in silica films. The optical

absorption spectra show no size dependence regarding the mean energy and the width of the plasmon band. Semi-quantal simulations using DFT and TD-LDA in the frame of the jellium model, including background and environment dielectric media, reproduce the experimental observations and permit disentangling the various contributions to the optical response. The constant spectral peak position, on the one hand, is rationalized as due to the impact of the porous effective dielectric environment on the balance between red-shift (spill-out) and blue-shift (layer of reduced d-electron polarizability at the interface). The width of the experimentally observed LSPR bands, on the other hand, is attributed mainly to inhomogeneous effects, i.e. variations in local environment. These become more important for smaller sizes and compensate the spectral narrowing due to the reduced number of electrons participating in the resonance.

Our combined experimental and theoretical study not only presents a comprehensive description of a complex nanoscale many-electron system but supplies the necessary tools for the conceptual comprehension of the transition between collective and molecular responses in small metal clusters, and thus also of the size-dependent metal-insulator transition. Notably we identify three parts in the electronic Hamiltonian: firstly, the electronic center-of-mass movement responsible for the surface plasmon resonance, secondly the internal single-electron excitations and thirdly the coupling between these two as mediated by the anharmonic character of the electron-jellium interaction potential. With decreasing cluster size this third term leads to a spectral fragmentation of the optical density (Landau damping). We identify chemical interactions (covalent bonds, oxidation) as decisive for the disappearance of the LSPR and thus of the metallic character. This is, however, no contradiction to narrow molecular-like transition leading to fluorescence, as sometimes observed for small silver clusters in different chemical surroundings.

We furthermore demonstrate that the conceptually simple jellium description of small metal clusters satisfactorily reproduces all size and effective environmental effects and provides the missing link between ab-initio approaches such as TD-DFT and effective solid-state models like Mie theory.

Solid oxide matrices provide weakly perturbing environments for such metal clusters and thereby allow identifying collective plasmonic responses for sizes much smaller than what is reported in the literature on ligand-stabilized particles. This underlines that great care has to be taken in the correct description of the electrons participating in either the delocalized and collective response or in localized covalent bonds at the metal-ligand interface.

ASSOCIATED CONTENT

Supporting Information. The supporting information discuss the different theoretical descriptions of the alumina matrix used for this work and their comparison with gas phase data. All simulated spectra are shown.

ACKNOWLEDGMENT

This work was supported by the French National Research Agency (ANR) via the projects 'FIT SPRINGS', ANR-14-CE08-0009 and 'SchNAPSS', ANR-21-CE09-0021. Further support by the French Campus France Eiffel Excellency Scholarship Program (EIFFEL-DOCTORAT

2020/P760767) for M.M. is acknowledged. The samples were elaborated at the PLYRA@iLMtech facility with technical support from C. Albin, C. Clavier and S. Hermelin.

REFERENCES

[1] Kreibig, U. and Vollmer, M. *Optical properties of metal clusters*. Springer series in materials science. Springer Berlin, (1995).

[2] Oyarzún, S., Tamion, A., Tournus, F., Dupuis, V., and Hillenkamp, M. Size effects in the magnetic anisotropy of embedded cobalt nanoparticles: from shape to surface. *Sci. Rep.* **5**, 14749 (2015).

[3] Serrano-Guisan, S., Di Domenicantonio, G., Abid, M., Abid, J.-P., Hillenkamp, M., Gravier, L., Ansermet, J.-P., and Félix, C. Enhanced magnetic field sensitivity of spin-dependent transport in cluster-assembled metallic nanostructures. *Nat. Mater.* **5**, 730 (2006).

[4] Heiz, U. and Landman, U. E., editors. *Nanocatalysis*. Springer, (2007).

[5] Odom, T. W. and Schatz, G. C. Introduction to Plasmonics. *Chem. Rev.* **111**(6), 3667–3668 (2011).

[6] Anker, J. N., Hall, W. P., Lyandres, O., Shah, N. C., Zhao, J., and Van Duyne, R. P. Biosensing with plasmonic nanosensors. *Nat. Mater.* **7**, 442–453 (2008).

[7] Sanchez, A., Abbet, S., Heiz, U., Schneider, W.-D., Hakkinen, H., Barnett, R., and Landman, U. When Gold Is Not Noble: Nanoscale Gold Catalysts. *J. Phys. Chem. A* **103**, 9573 (1999).

[8] Campos, A., Troc, N., Cottancin, E., Pellarin, M., Weissker, H.-C., Lermé, J., Kociak, M., and Hillenkamp, M. Plasmonic Quantum Size Effects in Silver Nanoparticles are Dominated by Interfaces and Local Environments. *Nat. Phys.* **15**, 275–280 (2019).

[9] Jin, R. Atomically precise metal nanoclusters: stable sizes and optical properties. *Nanoscale* **7**(5), 1549–1565 (2015).

[10] Amendola, V., Pilot, R., Frasconi, M., Maragò, O. M., and Iat, M. A. Surface plasmon resonance in gold nanoparticles: a review. *J. Phys.: Condens. Matter* **29**, 203002 (2017).

[11] Negishi, Y., Nakazaki, T., Malola, S., Takano, S., Niihori, Y., Kurashige, W., Yamazoe, S., Tsukuda, T., and Häkkinen, H. A Critical Size for Emergence of Nonbulk Electronic and Geometric Structures in Dodecanethiolate-Protected Au Clusters. *J. Am. Chem. Soc.* **137**, 1206–1212 (2015).

[12] Sakthivel, N. A., Theivendran, S., Ganeshraj, V., Oliver, A. G., and Dass, A. Crystal Structure of Faradaurate-279: Au_{279}(SPh-*t*Bu)$_{84}$ Plasmonic Nanocrystal Molecules. *J. Am. Chem. Soc.* **139**, 15450–15459 (2017).

[13] Zhou, M., Higaki, T., Li, Y., Zeng, C., Li, Q., Sfeir, M. Y., and Jin, R. Three-Stage Evolution from Nonscalable to Scalable Optical Properties of Thiolate-Protected Gold Nanoclusters. *J. Am. Chem. Soc.* **141**, 19754–19764 (2019).

[14] Yu, C., Harbich, W., Sementa, L., Ghiringhelli, L., Aprá, E., Stener, M., Fortunelli, A., and Brune, H. Intense fluorescence of Au_{20}. *J. Chem. Phys.* **147**, 074301 (2017).

[15] Yu, C., Schira, R., Brune, H., von Issendorff, B., Rabilloud, F., and Harbich, W. Optical properties of size selected neutral Ag clusters: electronic shell structures and the surface plasmon resonance. *Nanoscale* **10**, 20821–20827 (2018).

[16] von Issendorff, B. and Cheshnovsky, O. Metal To Insulator Transitions In Clusters. *Annu. Rev. Phys. Chem.* **56**, 549–580 (2005).

[17] Guryanov, I., Polo, F., Ubyvovk, E. V., Korzhikova-Vlakh, E., Tennikova, T., Rad, A. T., Nieh, M.-P., and Maran, F. Polylysine-grafted Au_{144} nanoclusters: birth and growth of a healthy surface-plasmon-resonance-like band. *Chem. Sci.* **8**, 3228–3238 (2017).

[18] Rambukwella, M., Sakthivel, N. A., Delcamp, J. H., Sementa, L., Fortunelli, A., and Dass, A. Ligand Structure Determines Nanoparticles' Atomic Structure, Metal-Ligand Interface and Properties. *Front. Chem.* **6**, 1 (2018).

[19] Xie, Y.-P., Shen, Y.-L., Duan, G.-X., Han, J., Zhang, L.-P., and Lu, X. Silver nanoclusters: synthesis, structures and photoluminescence. *Mater. Chem. Front.* **4**, 2205–2222 (2020).

[20] Sinha-Roy, R., López-Lozano, X., Whetten, R. L., and Weissker, H.-C. Crucial Role of Conjugation in Monolayer-Protected Metal Clusters with Aromatic Ligands: Insights from the Archetypal $Au_{144}L_{60}$ Cluster Compounds. *J. Phys. Chem. Lett.* **12**, 9262–9268 (2021).

[21] Hillenkamp, M., Di Domenicantonio, G., and Félix, C. Monodispersed metal clusters in solid matrices: A new experimental setup. *Rev. Sci. Instrum.* **77**, 025104 (2006).

[22] Haberland, H., Mall, M., Moseler, M., Qiang, Y., Reiners, T., and Thurner, Y. Filling of micron-sized contact holes with copper by energetic cluster impact. *J. Vac. Sci. Technol. A* **12**, 2925–2930 (1994).

[23] Bromann, K., Félix, C., Brune, H., Harbich, W., Monot, R., Buttet, J., and Kern, K. Controlled Deposition of Size-Selected Silver Nanoclusters. *Science* **274**, 956–958 (1996).

[24] Palpant, B., Prével, B., Lermé, J., Cottancin, E., Pellarin, M., Treilleux, M., Perez, A., Vialle, J. L., and Broyer, M. Optical properties of gold clusters in the size range 2-4 nm. *Phys. Rev. B* **57**, 1963 (1998).

[25] Lermé, J., Palpant, B., Prével, B., Pellarin, M., Treilleux, M., Vialle, J. L., Perez, A., and Broyer, M. Quenching of the Size Effects in Free and Matrix-Embedded Silver Clusters. *Phys. Rev. Lett.* **80**(23), 5105–5108 (1998).

[26] Lermé, J. Introduction of quantum finite-size effects in the Mie's theory for a multilayered metal sphere in the dipolar approximation: Application to free and matrix-embedded noble metal clusters. *Eur. Phys. J. D* **10**(2), 265–277 (2000).

[27] Cottancin, E., Celep, G., Lermé, J., Pellarin, M., Huntzinger, J. R., Vialle, J. L., and Broyer, M. Optical Properties of Noble Metal Clusters as a Function of the Size: Comparison between Experiments and a Semi-Quantal Theory. *Theor. Chem. Acc.* **116**, 514 (2006).

[28] Liebsch, A. Surface-plasmon dispersion and size dependence of Mie resonance: Silver versus simple metals. *Phys. Rev. B* **48**, 11317–11328 Oct (1993).

[29] Fedrigo, S., Harbich, W., and Buttet, J. Collective dipole oscillations in small silver clusters embedded in rare-gas matrices. *Phys. Rev. B* **47**, 10706–10715 (1993).

[30] Palik, E. *Handbook of Optical Constants of Solids*. Academic, New York, (1985).

[31] Lermé, J., Palpant, B., Prével, B., Cottancin, E., Pellarin, M., Treilleux, M., Vialle, J. L., Perez, A., and Broyer, M. Optical properties of gold metal clusters: A time-dependent local-density-approximation investigation. *Eur. Phys. J. D* **4**(1), 95–108 (1998).

[32] Johnson, P. B. and Christy, R. W. Optical Constants of the Noble Metals. *Phys. Rev. B* **6**, 4370–4379 (1972).

[33] Baida, H., Billaud, P., Marhaba, S., Christofilos, D., Cottancin, E., Crut, A., Lermé, J., Maioli, P., Pellarin, M., Broyer, M., Del Fatti, N., Vallée, F., Sánchez-Iglesias, A., Pastoriza-Santos, I., and Liz-Marzán, L. M. Quantitative Determination of the Size Dependence of Surface Plasmon Resonance Damping in Single Ag@SiO_2 Nanoparticles. *Nano Letters* **9**(10), 3463–3469 (2009).

[34] Lecoultre, S., Rydlo, A., Buttet, J., Félix, C., Gilb, S., and Harbich, W. Ultraviolet-visible absorption of small silver clusters in neon: Ag_n (n = 1-9). *J. Chem. Phys.* **134**, 184504 (2011).

[35] Genzel, L., Martin, T. P., and Kreibig, U. Dielectric function and plasma resonances of small metal particles. *Z. Phys. B* **21**, 339–46 (1975).

[36] Hillenkamp, M., Di Domenicantonio, G., Eugster, O., and Félix, C. Instability of Ag nanoparticles in SiO_2 at ambient conditions. *Nanotechnology* **18**, 015702 (2007).

[37] Lermé, J. Size Evolution of the Surface Plasmon Resonance Damping in Silver Nanoparticles: Confinement and Dielectric Effects. *J. Phys. Chem. C* **115**(29), 14098–14110 (2011).

[38] Sahoo, K. and Chakraborty, I. Ligand effects on the photoluminescence of atomically precise silver nanoclusters. *Nanoscale* **15**, 3120–3129 (2023).

[39] Bakr, O., Amendola, V., Aikens, C., Wenseleers, W., Li, R., Dal Negro, L., Schatz, G., and Stellacci, F. Silver Nanoparticles with Broad Multiband Linear Optical Absorption. *Angew. Chem.* **48**, 5921–5926 (2009).

[40] Chakraborty, I., Erusappan, J., Govindarajan, A., Sugi, K. S., Udayabhaskararao, T., Ghosh, A., and Pradeep, T. Emergence of metallicity in silver clusters in the 150 atom regime: a study of differently sized silver clusters. *Nanoscale* **6**, 8024–8031 (2014).

[41] Schira, R. and Rabilloud, F. Oxidation-Induced Surface Plasmon Band Fragmentation in Silver Clusters. *J. Phys. Chem. C* **124**(1), 968–975 (2020).

[42] Tiggesbäumker, J., Köller, L., Meiwes-Broer, K.-H., and Liebsch, A. Blue shift of the Mie plasma frequency in Ag clusters and particles. *Phys. Rev. A* **48**, R1749–R1752 (1993).

[43] Kasperovich, V. and Kresin, V. V. Ultraviolet photoabsorption spectra of silver and gold nanoclusters. *Phil. Mag.* **78**, 385–396 (1998).

[44] Loginov, E., Gomez, L. F., Chiang, N., Halder, A., Guggemos, N., Kresin, V. V., and Vilesov, A. F. Photoabsorption of Ag_N (N~6-6000) Nanoclusters Formed in Helium Droplets: Transition from Compact to Multicenter Aggregation. *Phys. Rev. Lett.* **106** (2011).

[45] Scholl, J. A., Koh, A. L., and Dionne, J. A. Quantum plasmon resonances of individual metallic nanoparticles. *Nature* **483**, 421–428 (2012).

[46] Raza, S., Stenger, N., Kadkhodazadeh, S., Fischer, S. V., Kostesha, N., Jauho, A.-P., Burrows, A., Wubs, M., and Mortensen, N. A. Blueshift of the surface plasmon resonance in silver nanoparticles studied with EELS. *Nanophotonics* **2**, 131–138 (2013).

[47] Lünskens, T., Heister, P., Thamer, M., Walenta, C. A., Kartouzian, A., and Heiz, U. Plasmons in supported size-selected silver nanoclusters. *Phys. Chem. Chem. Phys.* **17**, 17541–17544 (2015).

[48] Weissker, H.-C. and Lopez-Lozano, X. Surface plasmons in quantum-sized noble-metal clusters: TDDFT quantum calculations and the classical picture of charge oscillations. *Phys. Chem. Chem. Phys.* **17**, 28379–28386 (2015).

[49] Schira, R. and Rabilloud, F. Localized Surface Plasmon Resonance in Free Silver Nanoclusters Ag_n, n = 20–147. *J. Phys. Chem. C* **123**, 6205–6212 (2019).

[50] Lermé, J., Bonnet, C., Lebeault, M.-A., Pellarin, M., and Cottancin, E. Surface Plasmon Resonance Damping in Spheroidal Metal Particles: Quantum Confinement, Shape, and Polarization Dependences. *J. Phys. Chem. C* **121**(10), 5693–5708 (2017).

[51] Benoit, M., Puibasset, J., Bonafos, C., and Tarrat, N. Silica-induced electron loss of silver nanoparticles. *Nanoscale* **14**, 7280–7291 (2022).

[52] Kreibig, U., Gartz, M., Hilger, A., and Neuendorf, R. Interfaces in nanostructures: optical investigations on cluster-matter. *Nanostruc. Mater.* **11**, 1335–42 (1999).